Hydrogeology Journal – Electronic Supplementary Material

Revealing vertical aquifer heterogeneity and hydraulic anisotropy by pumping partially penetrating wells

Ruth Maier, Center for Applied Geoscience, University of Tübingen, Schnarrenbergstraße 94-96, 72076 Tübingen, Germany, ruth.maier@uni-tuebingen.de

Carsten Leven, Center for Applied Geoscience, University of Tübingen, Schnarrenbergstraße 94-96, 72076 Tübingen, Germany, carsten.leven-pfister@uni-tuebingen.de

Emilio Sánchez-León, Center for Applied Geoscience, University of Tübingen, Schnarrenbergstraße 94-96, 72076 Tübingen, Germany, emilio.sanchez@uni-tuebingen.de

Daniel Strasser, Federal Waterways Engineering and Research Institute, Kußmaulstraße 17, 76187 Karlsruhe, Germany, daniel.strasser@baw.de

Maximilian Stoll, Center for Applied Geoscience, University of Tübingen, Schnarrenbergstraße 94-96, 72076 Tübingen, Germany, maximilian.stoll@student.uni-tuebingen.de

Olaf A. Cirpka, **Corresponding author**, Center for Applied Geoscience, University of Tübingen, Schnarrenbergstraße 94-96, 72076 Tübingen, Germany, olaf.cirpka@uni-tuebingen.de

Section S1. Table S1 Key Data of the Monitoring Network

	R01	Nested observation wells north	Nested observation wells east	Nested observation wells south	Nested observation wells west
Purpose of well	Pumping well	Observation well	Observation well	Observation well	Observation well
Well type	Large-diameter well	Well bundle of three piezometers	Multi-channel tubing well	Well bundle of three piezometers	Well bundle of three piezometers
Diameter [m]	0.8	0.0254	0.01 per channel	0.0254	0.0254
Number of screens	3	3	7	3	3
Length of screen sections [m]	2	0.3	Channel 1-6: 0.4 Channel 7: 0.15	0.3	0.3
Distance r- and elevation from aquifer base z [m]	*r→* *0* *z↓* 37.3 30.8 24.3	*r→* *3.4* *6.5* *9.4* *10.4* *z↓* 35.4 35.3 35.2 32.2 32.3 32.5 28.5 29.3 30.6	*r→* *3.3* *6.8* *10.7* *20.9* *z↓* 39.1 38.9 38.9 38.7 37.0 36.9 36.9 36.9 33.8 33.1 33.9 33.9 30.3 30.4 30.4 30.6 26.8 27.1 27.1 27.9 23.8 23.9 24.0 23.9 21.0 20.9 20.9 20.8	*r→* *3.6* *6.3* *10.4* *z↓* 35.3 35.8 35.5 32.4 31.5 32.7 28.5 28.6 28.7	*r→* *3.5* *6.2* *10.2* *21.0* *z↓* 35.8 35.3 35.4 35.6 32.3 32.4 32.4 32.2 28.3 28.4 28.5 27.9

Section S2. Instability of Pressure Transducers and Pumping Rate

Figure S1 shows exemplary datasets of what we have defined as defective datasets. Such datasets have been eliminated from further processing. In general, we excluded datasets showing a drawdown signal that evidently does not correspond to the true signal of pumping. As shown in Figure S1, the instability of pressure transducer recordings can be expressed differently, including a steady decrease of drawdown (lowermost blue and yellow drawdown curves in Figure S1), a continuous trend in drawdown (green drawdown curve in Figure S1) or no response to pumping at all.

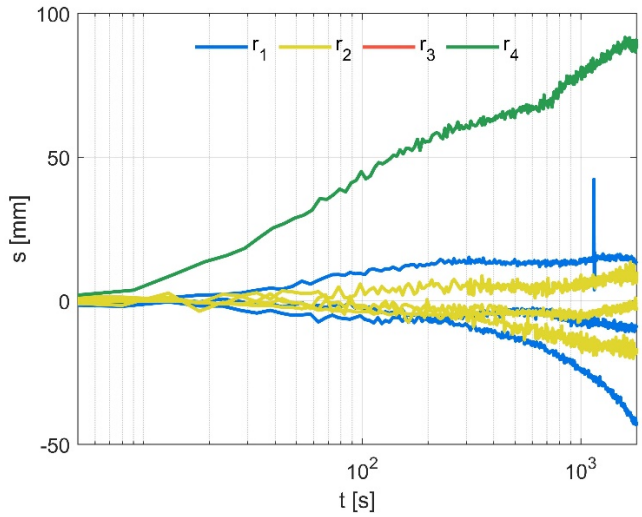

Figure S1. Datasets excluded from model calibration due to instable pressure transducer recordings.

With respect to flow rate stability, we assess the entire pumping phase including the late-term steady discharge. In preceding tests and during the main pumping tests, we have examined that the system shows an incredibly quick response to changes in the flow rate. Thus, we were able to identify flow rate instabilities not only directly from flow rate readings but also from observation data.

Section S3. Steady-Shape Pumping Regime

We consider the steady-shape pumping regime in which the absolute drawdowns are still changing but the hydraulic head differences between observation locations remain constant. We show an exemplary dataset to demonstrate the identification of the steady-shape pumping regime. Figure S2a shows the absolute drawdowns versus pumping time until timepoint t_{trim} = 1800 s obtained with pumping test $p_t = 5$ of hydraulic test I, i.e. when water was extracted from the upper screen. The drawdowns increase with time and decrease with increasing radial distance to the well (different colors in Figure S2a). Figure S2b shows the difference in drawdown between all observation points and observation point W04.3 chosen as an exemplary reference point. Contrary to the absolute drawdowns the drawdown differences appear to remain constant after a pumping time of ~15 min, that is, prior to the selected timepoint t_{trim}. To assess the change in drawdown we compute the logarithmic derivative (Figure S2c). Figure S2c indicates that the logarithmic derivative stabilizes prior to timepoint t_{trim} with differences smaller than 1 mm.

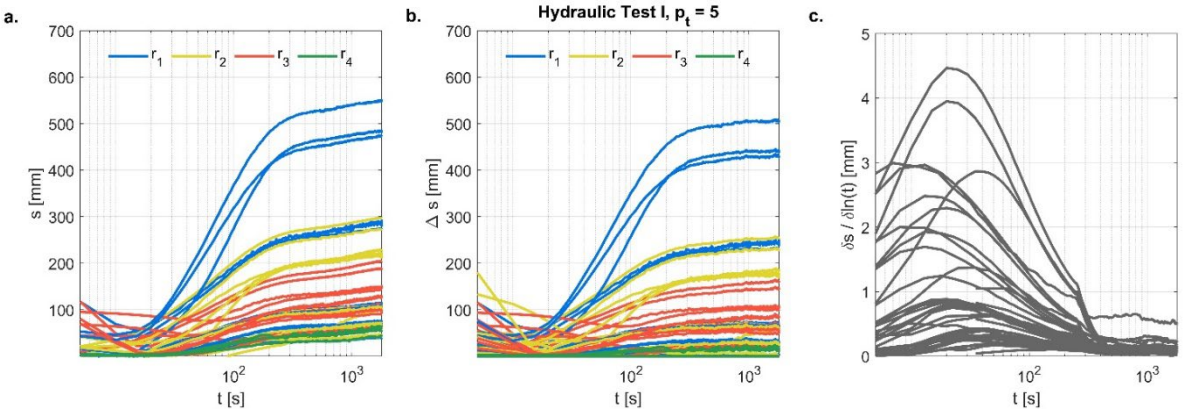

Figure S2. a. Absolute drawdown measurements versus pumping time. b. Drawdown differences between all observation points and observation point W04.3. c. Logarithmic derivative.

Section S4. Figure 7 of the main article in Log-Log Scale

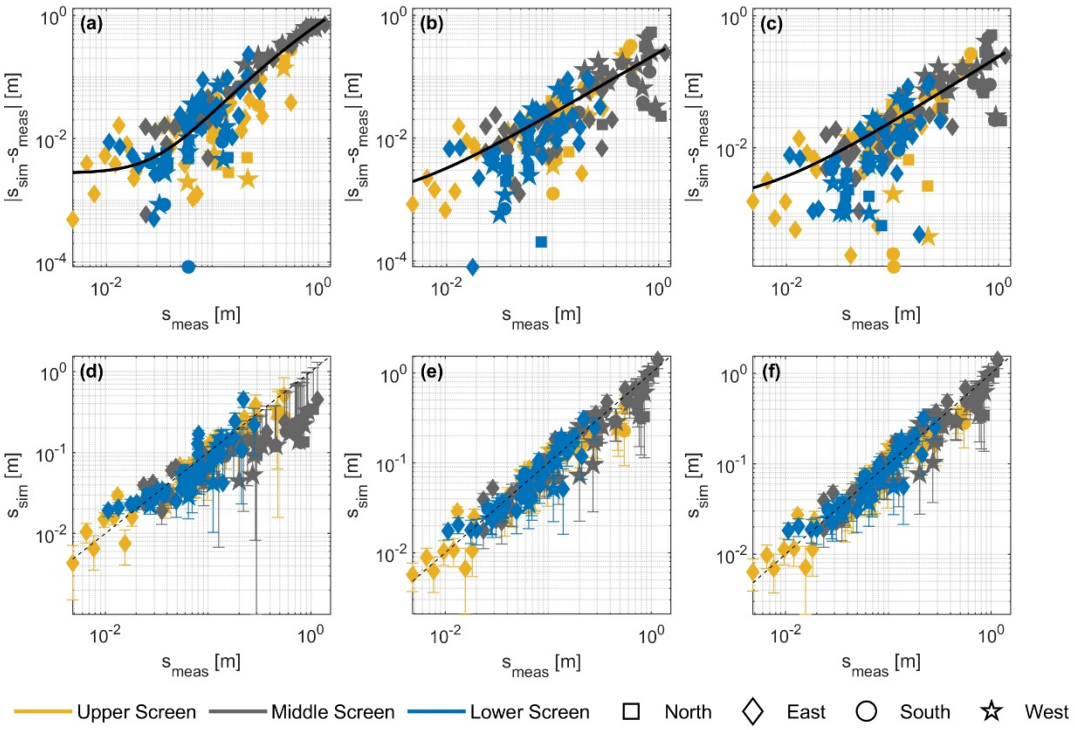

Figure S3. Assessment of model results. (a-c): Absolute difference between simulated and measured drawdown versus the measured drawdowns of the 1-layer model (a), 3-layer model (b), and 5-layer model (c) and the thereto fitted error models. (d-f): Field measurements versus simulated results of the best fitting 1-layer model (d), 3-layer model (e), and 5-layer model (f) with error-bars according to the error model. The black dashed diagonal lines represent the 1:1-identity lines.

Section S5. Assessing the Effective Conductivity Estimates

After model calibration we consider the effective conductivity estimates of the 5-layer model and feed these values to the 1-layer model. Figure S3 shows the resulting simulated drawdowns versus the measured drawdowns and the 1:1-identity line (black line in Figure S3). We compare the measurement fit of the 1-layer model when using the effective values from the 5-layer model (Figure S3) with the measurement fit based on the effective values resulting from the 1-layer model calibration (Figure S1c). Comparing Figure S3 and Figure S1c indicates that considering a homogeneous model with the effective conductivity estimates obtained from a multilayer model does not yield any improvement nor any deterioration in fitting the true drawdown measurements. This suggests that the effective horizontal hydraulic conductivity and effective vertical hydraulic conductivity are little informative when neglecting vertical differences of the hydraulic conductivity within the aquifer.

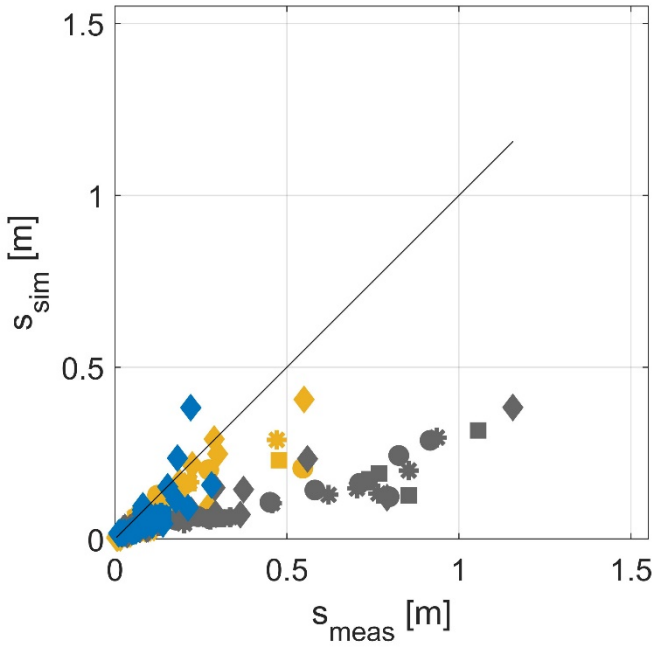

Figure S4. Simulated drawdowns versus measured drawdowns when running the 1-layer model with the effective conductivity estimates obtained from the 5-layer model calibration. The black diagonal line presents the 1:1-identity line.

Section S6. Markov-Chain Monte Carlo Results of Hydraulic Conductivity Values

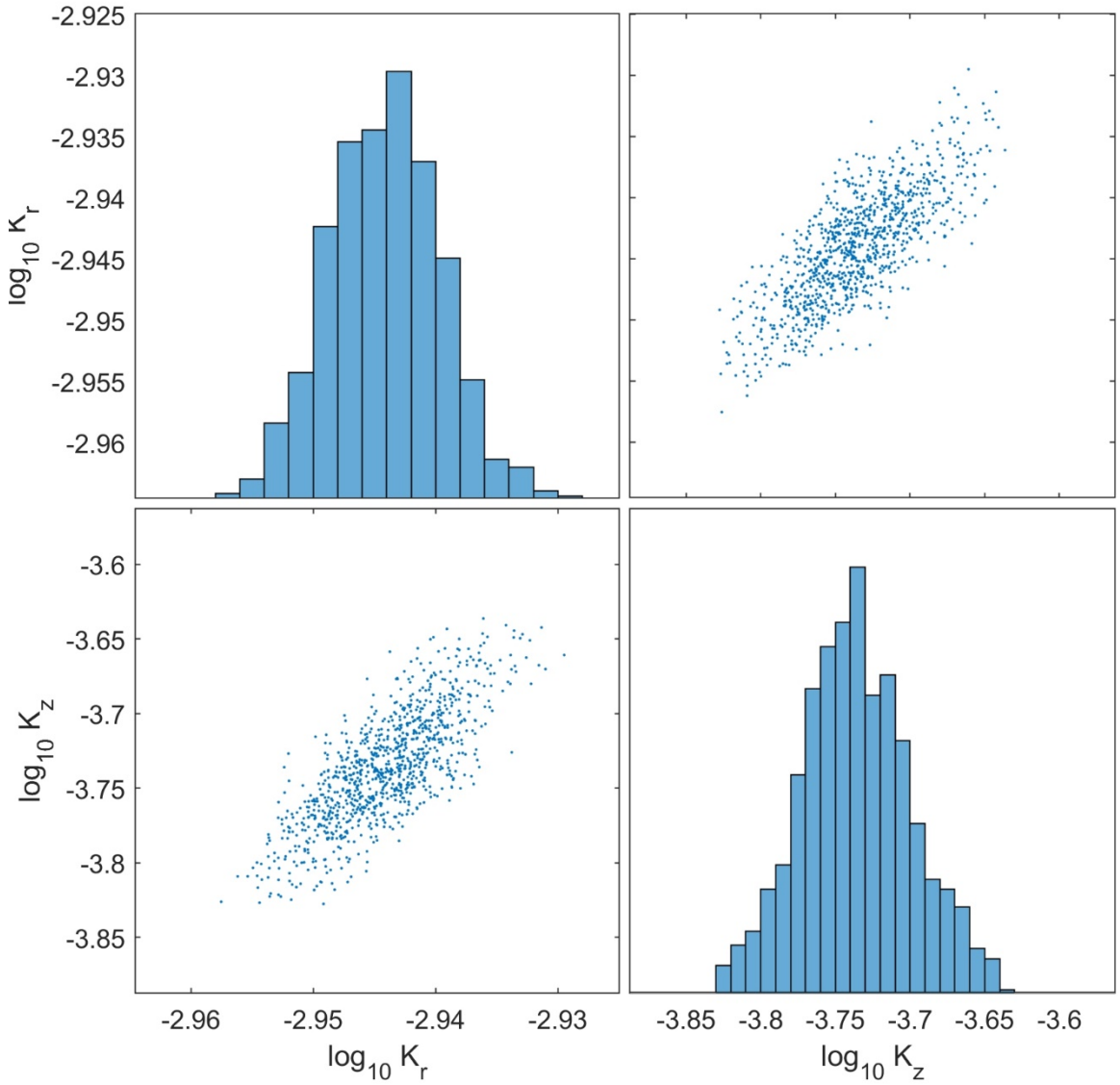

Figure S5. Pairwise scatter plots of hydraulic conductivity values in the MCMC sampling of the 1-layer model.

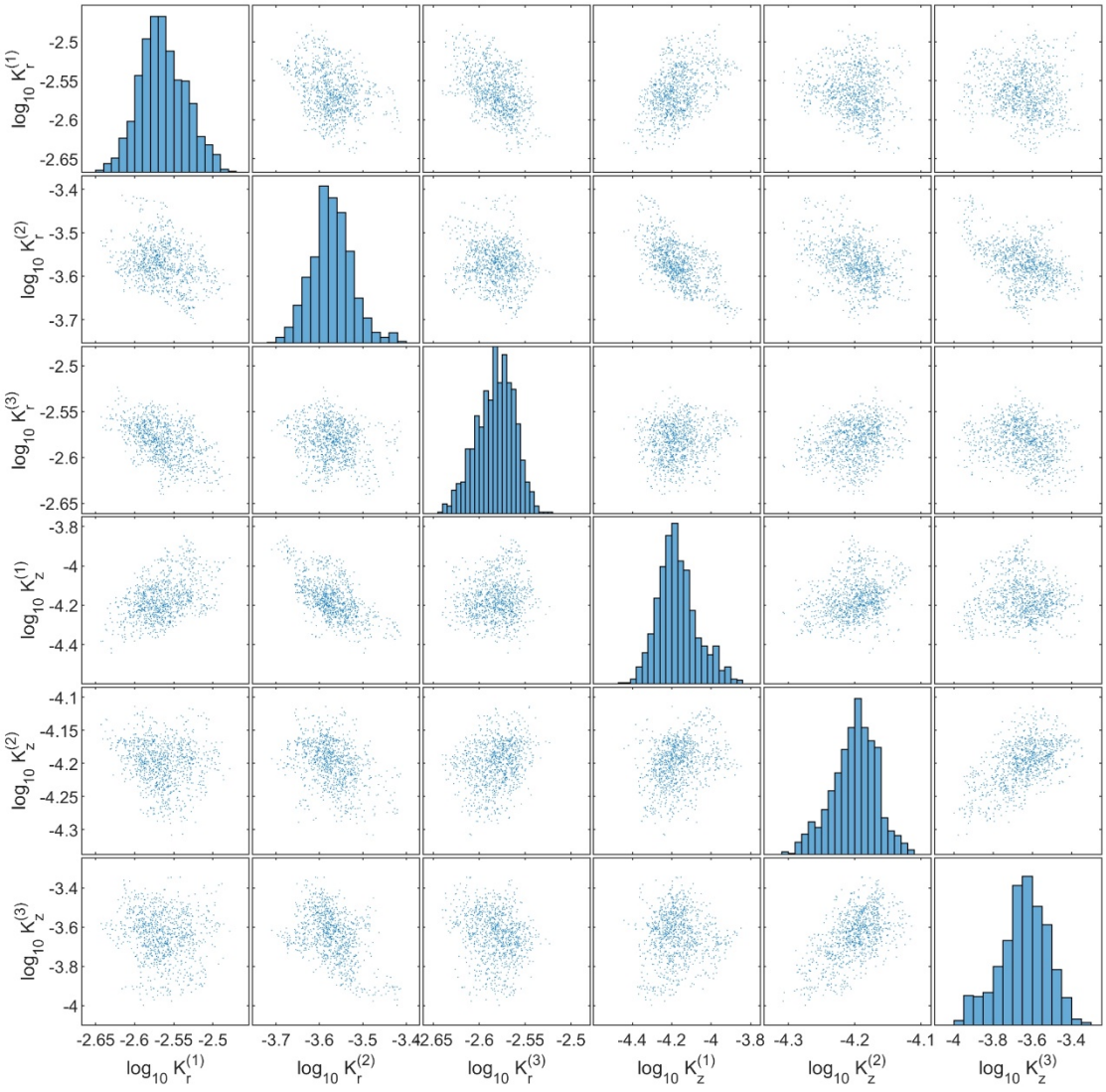

Figure S6. Pairwise scatter plots of hydraulic-conductivity values in the MCMC sampling of the 3-layer model.

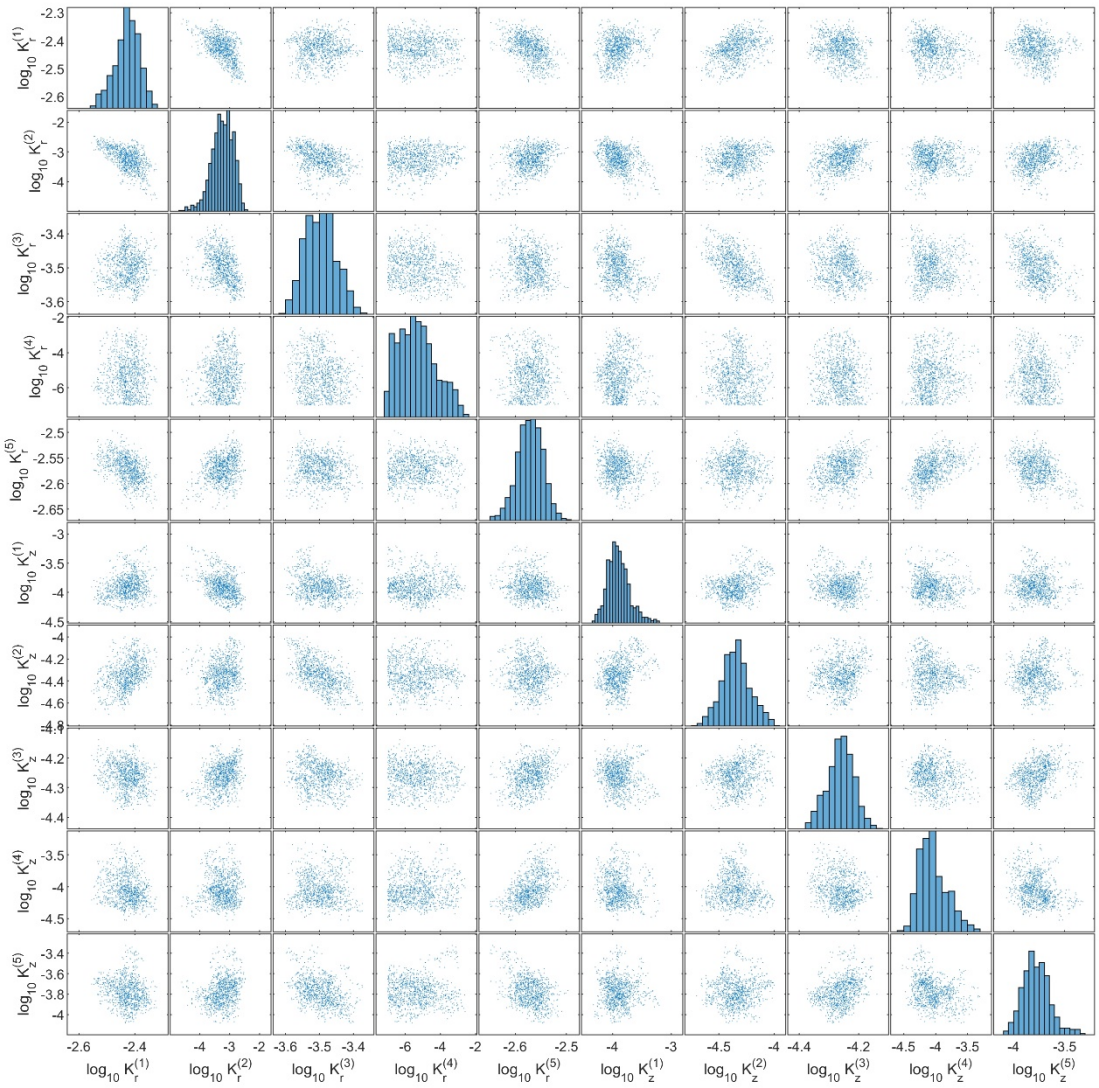

Figure S7. Pairwise scatter plots of hydraulic conductivity values in the MCMC sampling of the 5-layer model.